

Generalized Parton Distributions in Full Lattice QCD *

M. Göckeler^{1,2}, Ph. Hägler³, R. Horsley⁴, D. Pleiter⁵, P.E.L. Rakow⁶,
A. Schäfer², G. Schierholz⁷ and J.M. Zanotti⁵ (QCDSF collaboration)

¹Institut für Theoretische Physik, Universität Leipzig, D-04109 Leipzig, Germany

²Institut für Theoretische Physik, Universität Regensburg, D-93040 Regensburg, Germany

³Department of Physics and Astronomy, Vrije Universiteit, 1081 HV Amsterdam, NL

⁴School of Physics, University of Edinburgh, Edinburgh EH9 3JZ, UK

⁵John von Neumann-Institut für Computing NIC / DESY, D-15738 Zeuthen, Germany

⁶Theoretical Physics Division, Dep. of Math. Sciences, University of Liverpool,
Liverpool L69 3BX, UK

⁷Deutsches Elektronen-Synchrotron DESY, D-22603 Hamburg, Germany

Abstract. We present recent results on generalized parton distributions from dynamical lattice QCD calculations. Our set of twelve different combinations of couplings and quark masses allows for a preliminary study of the pion mass dependence of the transverse nucleon structure.

1 Introduction

The investigation of the nucleon structure in the framework of QCD is a major task in today's particle physics. Generalized parton distributions (GPDs) have opened new ways of studying the complex interplay of longitudinal momentum and transverse coordinate space as well as spin and orbital angular momentum degrees of freedom in the nucleon. The twist-2 GPDs H , E , \tilde{H} and \tilde{E} of quarks in the nucleon are defined by the following parameterization of off-forward nucleon matrix elements

$$\langle P', \lambda' | \int \frac{d\lambda}{4\pi} e^{i\lambda x} \bar{\psi}(-\frac{\lambda}{2}n) \gamma^\mu \mathcal{U} \psi(\frac{\lambda}{2}n) | P, \lambda \rangle = \bar{U}(P', \lambda') \left(\gamma^\mu H(x, \xi, t) + \frac{i\sigma^{\mu\nu} \Delta_\nu}{2m} E(x, \xi, t) \right) U(P, \lambda), \quad (1)$$

for the helicity independent vector case, and

$$\langle P', \lambda' | \int \frac{d\lambda}{4\pi} e^{i\lambda x} \bar{\psi}(-\frac{\lambda}{2}n) \gamma_5 \gamma^\mu \mathcal{U} \psi(\frac{\lambda}{2}n) | P, \lambda \rangle = \bar{U}(P', \lambda') \left(\gamma_5 \gamma^\mu \tilde{H}(x, \xi, t) + \frac{\gamma_5 \Delta^\mu}{2m} \tilde{E}(x, \xi, t) \right) U(P, \lambda), \quad (2)$$

*Presented by Ph. Hägler at Light-Cone 2004, Amsterdam, 16 - 20 August

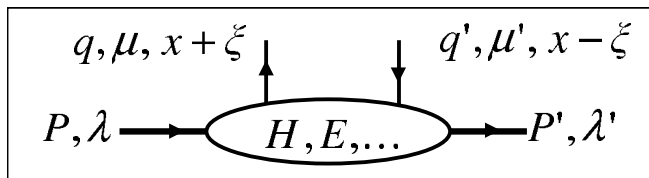


Figure 1. Graphical representation of GPDs as part of a scattering amplitude

for the helicity dependent axial vector case [1, 2, 3]. Wilson lines ensuring gauge invariance of the bilocal operators are denoted by \mathcal{U} . Here and in the following we do not show explicitly the dependence of the GPDs on the resolution scale Q^2 . Fig.(1) shows the definition of the particle momenta and helicities. The momentum transfer (squared) is given by $\Delta = P' - P$ ($t = \Delta^2$). Using the light cone vector n we define the longitudinal momentum transfer by $\xi = -n \cdot \Delta/2$. The proper definition of the twist-2 tensor or quark helicity flip GPDs H_T , E_T , \tilde{H}_T and \tilde{E}_T can be found in [4]. GPDs provide a solid framework in QCD to relate many different aspects of hadron physics:

- The forward limit $\Delta \rightarrow 0$ of certain GPDs reproduces the well known parton distributions, that is $H(x, \xi = 0, t = 0) = q(x) = f_1(x)$, $\tilde{H}(x, 0, 0) = \Delta q(x) = g_1(x)$ and $H_T(x, 0, 0) = \delta q(x) = h_1(x)$.
- The integral over the longitudinal momentum fraction $\int dx$ of the GPDs gives the Dirac, Pauli, axial, pseudo-scalar, tensor etc. form factors, $\int dx H(x, \xi, t) = F_1(t)$, $\int dx E = F_2(t)$, $\int dx \tilde{H} = g_A(t)$, $\int dx \tilde{E} = g_P(t)$, $\int dx H_T = g_T(t)$ etc.
- The Fourier transforms $\int d\Delta_\perp e^{-ib_\perp \cdot \Delta_\perp}$ of the GPDs H , \tilde{H} and H_T at $\xi = 0$ are coordinate space probability densities in the impact parameter b_\perp [5].
- The forward limit of the x -moment of the GPD E , $\int dx x E(x, 0, 0) = B_{20}(0)$, allows for the determination of the quark orbital angular momentum contribution to the nucleon spin, $L^q = 1/2(\langle x \rangle + B_{20} - \Delta q)$, where $\langle x \rangle$ is the quark momentum fraction.

The fact that the impact parameter dependent quark distributions like

$$q(x, b_\perp) \equiv \int d^2 \Delta_\perp e^{-ib_\perp \cdot \Delta_\perp} H(x, \xi = 0, t = -\Delta_\perp^2) \quad (3)$$

have the interpretation of probability densities in the transverse plane marks a major step forward in the understanding of the nucleon structure. A very interesting observation in this respect is that at large longitudinal momentum fraction, $x \rightarrow 1$, i.e. when the active parton carries the whole nucleon momentum and the spectators give only a negligible contribution, the active parton becomes the center of momentum of the nucleon at $R_\perp = 0$. Accordingly, the impact parameter profile of the nucleon will be strongly peaked at $b_\perp = 0$. Keeping in mind that the parton distributions eventually vanish in the limit $x \rightarrow 1$, we expect that $\lim_{x \rightarrow 1} q(x, b_\perp)/q(x) \propto \delta^2(b_\perp)$. Transferred to momentum space, we

#	1	2	3	4	5	6	7	8	9	10	11	12
β	5.20	5.20	5.20	5.25	5.25	5.25	5.29	5.29	5.29	5.40	5.40	5.40
κ	.13420	.13500	.13550	.13460	.13520	.13575	.13400	.13500	.13550	.13500	.13560	.13610
a[fm]	0.12	0.11	0.099	0.11	0.097	0.091	0.1	0.096	0.09	0.082	0.079	0.075
L[fm]	1.96	1.68	1.59	1.69	1.56	2.19	1.66	1.53	2.16	1.97	1.88	1.79
m_{π} [Gev]	0.94	0.777	0.578	0.92	0.774	0.553	1.09	0.867	0.716	0.969	0.788	0.588
$m_{\pi} \times L$	9.36	6.64	4.66	7.89	6.11	6.14	9.23	6.74	7.85	9.68	7.48	5.3

Figure 2. Some parameters of our calculation.

have the striking prediction that the normalized GPD $H(x, 0, t)/q(x)$ will be constant in the limit $x \rightarrow 1$ [6, 7].

Interesting recent results on GPDs using available experimental data on form factors and PDFs can be found in [8].

On the lattice side, we cannot deal directly with matrix elements of bilocal light-cone operators. Therefore we first transform the LHS in Eqs.(1,2) to Mellin space by integrating over x , i.e. $\int dx x^{n-1}$. This results in matrix elements of towers of local operators which are in turn parameterized in terms of so-called generalized form factors (GFFs) $A(t), B(t) \dots$,

$$\begin{aligned} \langle P', \lambda' | \bar{\psi}(0) \Gamma i \overleftrightarrow{D}^{\{\mu_1} \dots i \overleftrightarrow{D}^{\mu_n\}} \psi(0) | P, \lambda \rangle &= \overline{U}(P', \lambda') (a_{\Gamma}^{\mu_1 \dots \mu_n} A(t) \\ &+ b_{\Gamma}^{\mu_1 \dots \mu_n} B(t) + \dots) U(P, \lambda), \end{aligned} \quad (4)$$

where the subtraction of traces is implicit. The explicit parameterization for the tower of vector operators, $\Gamma \equiv \gamma^{\mu}$, is given in [9] in terms of the GFFs $A_{ni}(t), B_{ni}(t)$ and $C_{n0}(t)$. In the axial vector case, the corresponding expression in terms of the GFFs $\tilde{A}_{ni}(t)$ and $\tilde{B}_{ni}(t)$ is shown in [10]. Parameterizations for the tensor GPDs have been derived recently in [11, 12]. Having computed the GFFs in e.g. lattice QCD, it is fairly simple to get the moments of the corresponding GPDs by using the following polynomial relations [13]

$$\begin{aligned} H^n(\xi, t) &\equiv \int_{-1}^1 dx x^{n-1} H(x, \xi, t) = \sum_{i=0, \text{even}}^{n-1} (-2\xi)^i A_{ni}(t) + (-2\xi)^n C_{n0}(t)|_{n \text{ even}}, \\ E^n(\xi, t) &= \sum_{i=0, \text{even}}^{n-1} (-2\xi)^i B_{ni}(t) - (-2\xi)^n C_{n0}(t)|_{n \text{ even}}, \\ \tilde{H}^n(\xi, t) &= \sum_{i=0, \text{even}}^{n-1} (-2\xi)^i \tilde{A}_{ni}(t), \quad \tilde{E}^n(\xi, t) = \sum_{i=0, \text{even}}^{n-1} (-2\xi)^i \tilde{B}_{ni}(t). \end{aligned} \quad (5)$$

In the limit $\xi \rightarrow 0$, the complete nucleon structure related to H and \tilde{H} is according to Eq.(5) represented by the sets of GFFs $A_{n0}(t)$ and $\tilde{A}_{n0}(t)$, $n = 1 \dots \infty$.

2 Lattice results

The lattice calculation and extraction of the GFFs from nucleon two- and three-point-functions follows the standard procedure as outlined in e.g. [14, 15, 16].

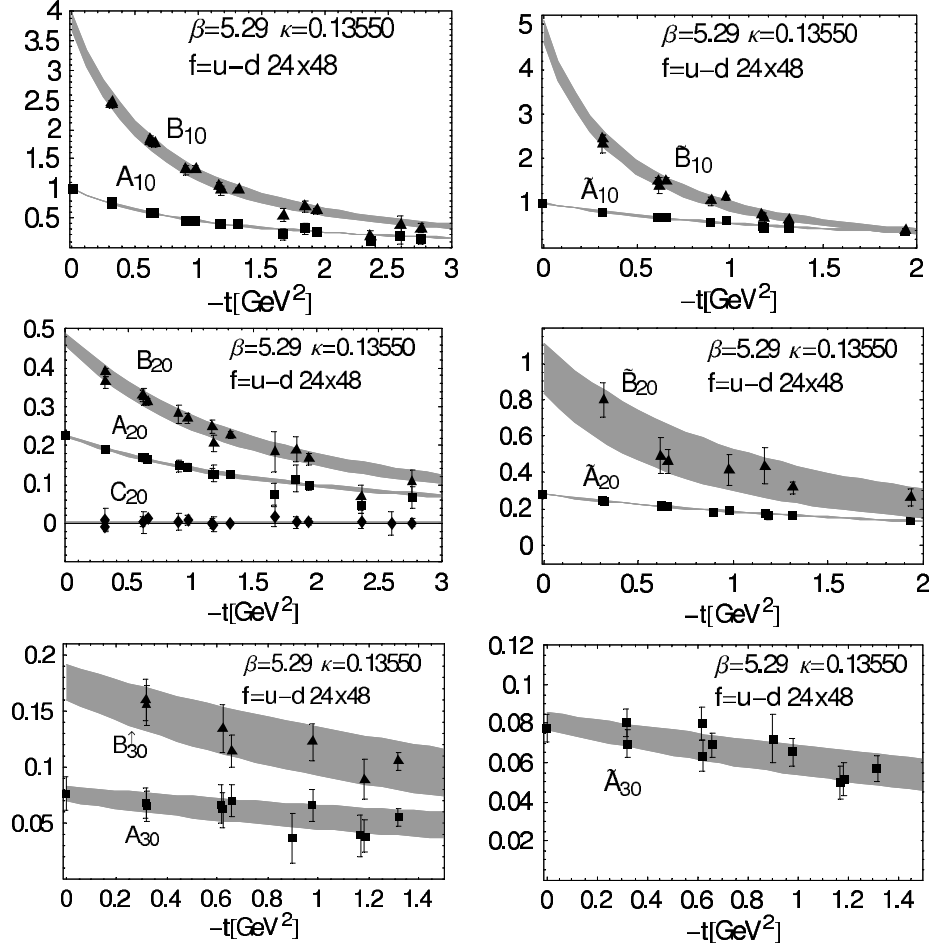


Figure 3. Lowest three moments of the GPDs $H(x, 0, t)$, $E(x, 0, t)$ (left column) and $\tilde{H}(x, 0, t)$, $\tilde{E}(x, 0, t)$ (right column).

Our dynamical computations are currently based on a set of coupling- and quark mass-combinations with up to $O(1200)$ configurations and with pion masses ranging from 1.1 down to 0.55 GeV. The lattice spacing lies in between ≈ 0.07 and ≈ 0.12 fm. Since we are using non-perturbatively $O(a)$ improved Wilson fermions, we do not expect strong discretization effects [16]. A list of the parameters is given in Fig.(2). We do not take into account the disconnected contributions which are numerically much harder to evaluate. This is irrelevant as long as we concentrate on the iso-vector channel $u-d$ (as we do here), for which the disconnected pieces would cancel due to iso-spin symmetry. To give an overview of our results we show in Fig.(3) the lowest three moments of the GPDs $H(x, 0, t)$, $E(x, 0, t)$ and $\tilde{H}(x, 0, t)$ as well as the lowest two moments of $\tilde{E}(x, 0, t)$. Up to now, only the lowest moments $n = 1$ which we show here are non-perturbatively renormalized, and operator mixing has to be taken into account for a proper renormalization of the x^2 -moments for $i > 0$ [17]. We do not expect the renor-

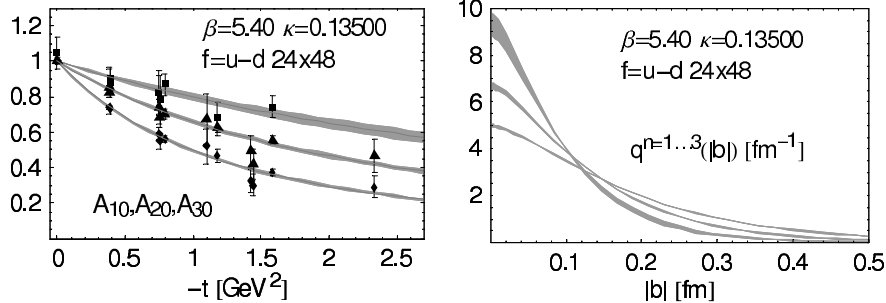


Figure 4. Change of slope of the GFFs (left) and narrowing of the corresponding b_{\perp} dependent GFFs (right); $n = 1$ corresponds to the lowest (widest) curve in the left(right)-hand plot.

malization to affect the following general discussion and the extraction of the dipole masses below. Please note that for reasons of clarity $B_{30}(t)$ has been shifted upwards by 0.05, as indicated by the superscript arrow in Fig.(3), lower left panel. All GFFs have been fitted using a standard dipole ansatz,

$$A_{ni}^{\text{dipole}}(t) = \frac{A_{ni}^{\text{dipole}}(0)}{(1 - t/m_D^2)^2}, \quad (6)$$

except for the pseudo-scalar FF $\tilde{B}_{10}(t) = g_P(t)$, where we used a dipole ansatz including the pion-pole,

$$\tilde{B}_{10}^{\pi\text{pole}}(t) = \frac{\tilde{B}_{10}^{\pi\text{pole}}(0)}{(1 - t/m_D^2)^2 (1 - t/m_{\pi}^2)}. \quad (7)$$

The fits given by the gray bands in Figs.(3) show an overall satisfactory description of the lattice numbers. While the statistical errors for the lowest two moments are rather small, they tend to be somewhat larger for the x^2 -moment. The statistics are particularly poor for A_{32} , \tilde{A}_{32} and the \tilde{B}_{3i} GFFs, which are not shown in this work. It turns out that the moments of H and \tilde{H} in the iso-vector channel are a factor of 2...5 smaller than the corresponding moments of E and \tilde{E} , while C_{20} which contributes to both H and E is compatible with zero. Our results indicate furthermore strong cancellations of u and d flavor contributions in the iso-singlet channel for the helicity independent GPD E^{u+d} .

Let us now take a look at the t -dependence of the GPDs and the impact parameter dependent quark distribution $q(x, b_{\perp})$. The observation from section (1) that $\lim_{x \rightarrow 1} H(x, 0, t)/q(x) = 1$ translates directly to the statement that the GFFs $A_{n0}(t)$ become constant for very large n since increasingly more weight lies on values of x close to one for $\lim_{n \rightarrow \infty}$. To be precise, we expect that $\lim_{n \rightarrow \infty} A_{n0}(t)/A_{n0}(0) = 1$, independent of t . Since the values for the momentum transfer squared in our computation are unevenly distributed in the interval $-3.5 < t < 0$ GeV, and since there is in particular a gap between $t = 0$ and the smallest non-zero t which can be realized on the given lattices, t_{\min} , it is not useful to perform a discrete Fourier transformation (FT) of our results to impact

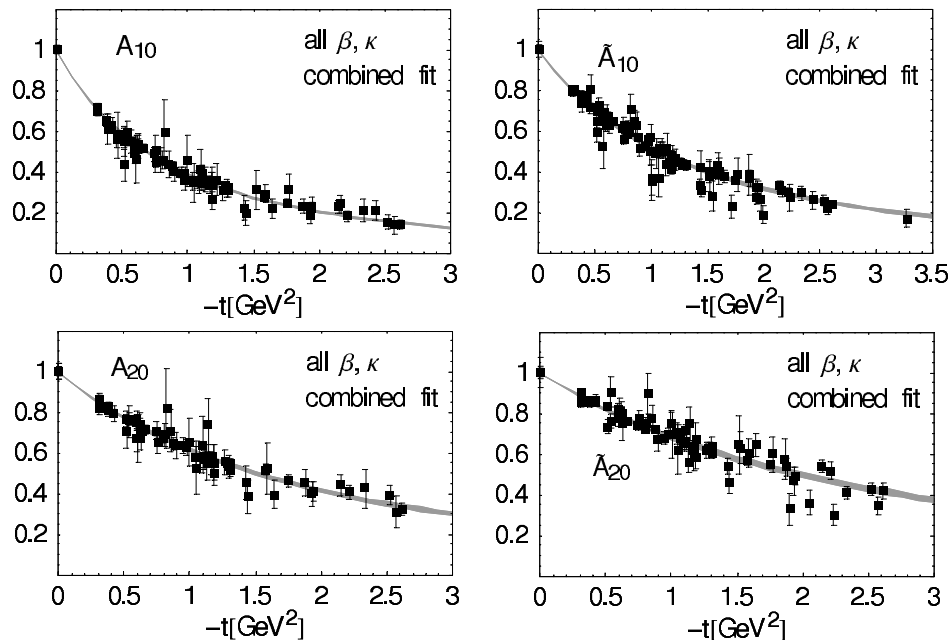


Figure 5. Joined results for all β, κ combinations for the lowest two moments of $H(x, 0, t)$ (left column) and $\tilde{H}(x, 0, t)$ (right column).

parameter space. Instead, we directly use the continuous FT of the dipole ansatz Eq.(6). The normalized impact parameter dependent moments $q^{n=1..3}(b_\perp)$ with $\int db_\perp q^{n=1..3}(b_\perp) = 1$ are shown in Fig.(4). For reasons of comparison we show in Fig.(4) also the corresponding GFFs, normalized to $A_{n0}^{\text{dipole}}(0) = 1$. The gray bands in the impact parameter plot reflect the errors associated with the dipole masses, Δm_D . The results in Fig.(4) show very nicely the anticipated flattening of the GFFs and the narrowing of the corresponding distributions in impact parameter space, going from $n = 1$ to $n = 3$. This flattening of the GPDs has first been observed in [18].

Since we have results for a large number of pion masses at hand, it is mandatory to concentrate in the following on the important issue of the m_π dependence and the chiral extrapolation of our calculation. Due to the use of Wilson fermions, the dominant part of our computation is for pion masses above 600 MeV where chiral perturbation theory in its current form is most probably not applicable. In particular for the dipole masses m_D , we therefore resort to a purely phenomenologically motivated pion mass dependence of the form $m_D = m_D^0 + \alpha m_\pi^2$. We have checked that a linear dependence on m_π is clearly unfavored by our results. For the following analysis we have normalized our results to $A_{n0}^{\text{dipole}}(0) = 1$ first. One option is then to perform dipole fits for all individual β, κ combinations for a given moment n and fit the pion mass dependence of the dipole masses with the given ansatz. However to optimally utilize the information on the dipole masses from our collection of results, it is better to use a combined

dipole-mass/pion-mass fit of the simple form

$$\bar{A}_{n0}^{\text{dipole},m_\pi}(t) = \frac{1}{(1 - t/(m_D^0 + \alpha m_\pi^2))^2}, \quad (8)$$

depending on the two parameters m_D^0 and α . Having done the fit, we may shift the raw numbers to a common curve given by Eq.(8) at the physical pion mass, $m_{\pi,\text{phys}} = 139$ MeV. The results of this procedure are shown in Fig.(5) for the GFFs A_{n0} and \tilde{A}_{n0} , $n = 1, 2$. The fit parameters are found to be

$$\begin{aligned} A_{10} & : m_D^0 = 1.27 \pm .01 \text{ GeV}, \quad \alpha = 0.29 \pm .02 \text{ GeV}^{-2} \\ A_{20} & : m_D^0 = 1.90 \pm .03 \text{ GeV}, \quad \alpha = 0.14 \pm .05 \text{ GeV}^{-2} \\ \tilde{A}_{10} & : m_D^0 = 1.59 \pm .02 \text{ GeV}, \quad \alpha = 0.16 \pm .03 \text{ GeV}^{-2} \\ \tilde{A}_{20} & : m_D^0 = 2.18 \pm .05 \text{ GeV}, \quad \alpha = -0.10 \pm .06 \text{ GeV}^{-2}. \end{aligned} \quad (9)$$

Although the corresponding rather large error does not allow for a definite conclusion, it is interesting to note that the slope α changes sign going from \tilde{A}_{10} to \tilde{A}_{20} . We observe an overall nice clustering of the lattice points in Fig.(5) much in favor of our ansatz Eq.(8). The actual fits are given by the gray bands and show a very good χ^2/NODOF lying below 0.2 for the helicity independent and below 0.5 for the helicity dependent case. In particular for \tilde{A}_{n0} , a small fraction of the lattice points seem to be significantly below the main line. Future investigations have to show if this is due to an unaccounted dependence on the lattice spacing, the (finite) lattice volume or just insufficient statistics. An attempt to compare our results for the axial and tensor coupling, $g_A(0)$ and $g_T(0)$, with chiral perturbation theory is described in [19]. We plan to extract the quark orbital angular momentum contribution to the nucleon spin as soon as the missing renormalization constants become available.

3 Conclusion

We have computed the lowest moments of GPDs for a number of different pion masses in the range above 550 MeV. The results are very well described by a combined dipole-mass/pion-mass fit. While we observe no sign of chiral logarithms in the available range of pion masses, let us note that first promising lattice calculations towards the chiral region are currently under way using overlap [20] as well as domain wall fermions [21].

Acknowledgments

The numerical calculations have been performed on the Hitachi SR8000 at LRZ (Munich), on the Cray T3E at EPCC (Edinburgh) and on the APEmille at NIC/DESY (Zeuthen). This work has been supported in part by the DFG (Forschergruppe Gitter-Hadronen-Phaenomenologie), the EU Integrated Infrastructure Initiative ‘‘Hadron Physics’’ as well as ‘‘Study of Strongly Interactive Matter’’ (in parts under contract number RII3-CT-2004-506078).

References

1. D. Müller, D. Robaschik, B. Geyer, F. M. Dittes and J. Horejsi, Fortsch. Phys. **42** (1994) 101 [arXiv:hep-ph/9812448].
2. X. D. Ji, Phys. Rev. D **55** (1997) 7114 [arXiv:hep-ph/9609381].
3. A. V. Radyushkin, Phys. Rev. D **56** (1997) 5524 [arXiv:hep-ph/9704207].
4. M. Diehl, Eur. Phys. J. C **19** (2001) 485 [arXiv:hep-ph/0101335].
5. M. Burkardt, Phys. Rev. D **62** (2000) 071503 [Erratum-ibid. D **66** (2002) 119903] [arXiv:hep-ph/0005108].
6. M. Burkardt, Int. J. Mod. Phys. A **18** (2003) 173 [arXiv:hep-ph/0207047].
7. M. Burkardt, Phys. Lett. B **595** (2004) 245 [arXiv:hep-ph/0401159].
8. M. Diehl, T. Feldmann, R. Jakob and P. Kroll, arXiv:hep-ph/0408173.
9. P. Hoodbhoy, X. D. Ji and W. Lu, Phys. Rev. D **59** (1999) 014013 [arXiv:hep-ph/9804337].
10. M. Diehl, Phys. Rept. **388** (2003) 41 [arXiv:hep-ph/0307382].
11. Ph. Hägler, Phys. Lett. B **594** (2004) 164 [arXiv:hep-ph/0404138].
12. Z. Chen and X. D. Ji, arXiv:hep-ph/0404276.
13. X. D. Ji, W. Melnitchouk and X. Song, Phys. Rev. D **56** (1997) 5511 [arXiv:hep-ph/9702379].
14. Ph. Hägler, J. Negele, D. B. Renner, W. Schroers, T. Lippert and K. Schilling [LHPC collaboration], Phys. Rev. D **68** (2003) 034505 [arXiv:hep-lat/0304018].
15. M. Göckeler, R. Horsley, D. Pleiter, P. E. L. Rakow, A. Schäfer, G. Schierholz and W. Schroers [QCDSF Collaboration], Phys. Rev. Lett. **92** (2004) 042002 [arXiv:hep-ph/0304249].
16. M. Göckeler *et al.*, arXiv:hep-lat/0409162.
17. M. Göckeler, R. Horsley, H. Perlt, P. E. L. Rakow, A. Schäfer, G. Schierholz and A. Schiller, arXiv:hep-lat/0409025; arXiv:hep-lat/0410009.
18. Ph. Hägler, J. W. Negele, D. B. Renner, W. Schroers, T. Lippert and K. Schilling [LHPC], Phys. Rev. Lett. **93** (2004) 112001 [arXiv:hep-lat/0312014].
19. A. Ali Khan *et al.*, arXiv:hep-lat/0409161.
20. M. Gürtler *et al.*, arXiv:hep-lat/0409164.
21. D. B. Renner *et al.* [LHPC], arXiv:hep-lat/0409130